Strain versus Dislocation Model for Understanding the Heteroepitaxial Growth of Nanowires

Jian Shi and Xudong Wang*

Department of Materials Science and Engineering, University of Wisconsin at Madison, Madison, Wisconsin 53706

Received: November 2, 2009; Revised Manuscript Received: December 17, 2009

In this paper, we adapted the Stranski-Krastanow (SK) mode to the heteroepitaxial growth of NWs and suggested three general growth modes (SK, island SK, and coherent SK) covering all phenomena observed from nanostructures epitaxially grown on single crystal substrates. A strain versus dislocation (SVD) model was also established to define these three modes. The SVD model analyzes the competition between strain energy and dislocation energy at the NW-substrate interface. Experimental data acquired from ZnO NWs grown on GaN substrates via the three modes exhibited a good match to our theoretical prediction. NWs could be grown coherently on the substrate only when their sizes are smaller than the critical size. A defective intermediate structure was found to be necessary for growing nanostructures larger than the critical sizes. The SVD model has also been successfully applied to ZnO nanofins grown on GaN and ZnO NWs grown on sapphire, which demonstrated the generality of the SVD model for understanding the heteroepitaxial growth behaviors of various nanostructures. This work provided a necessary quantitative complement to the thermodynamics and diffusion kinetics in predicting the nanostructure growth phenomena.

1. Introduction

Semiconductor nanowires (NWs) are considered as an important building block for advanced electronic and optoelectronic devices including light-emitting diodes,[1,2] solid state lasers,[3,4] transistors,[5–8] transducers,[6,9,10] solar cells,[11,12] and nanogenerators.[13,14] Growing aligned NWs epitaxially on single crystal substrates has shown great promises for characterizing their properties[9] and designing/fabricating novel NW-based nanodevices.[15,16] The aligned NW configuration would potentially offer higher performance comparing to conventional 2D thin film devices.[17] In most cases, the supporting substrates are different materials from the NWs due to the substrate availability or application demands. For example, heterjunctions between NWs and substrate are needed for constructing diodes with designed band alignment.[2,5] Typical aligned-NW-on-heterogeneous-substrate systems include Ge, InAs NWs on Si substrates,[16] ZnO NWs on GaN, AlN, SiC or sapphire substrates,[18] InAs NWs on GaAs or InGaAs substrates,[19] GaN NWs on SiC substrates,[20] and so on. How to grow uniform, well controlled, and perfectly aligned NW arrays from desired materials is the ultimate goal of NW synthesis. Understandings have been established on catalyst effects[21–23] and kinetic parameters such as precursor and catalyst atom diffusion.[22,24,25] However, in reality, the size of NWs may not be always determined by the size of catalyst. Diffusion kinetics and thermodynamic equilibrium may not be sufficient to predict all the NW epitaxial growth phenomena, such as the automatic formation of a buffer layer beneath NW arrays under certain circumstance.[26] It is believed that the small lattice mismatch between the NWs and the substrate may be another significant parameter dictating those phenomena. Although a little theoretical work has been performed to explain the heteroepitaxial junctions between NWs,[27–29] a more general model is greatly desired to bridge the theoretical prediction and the NW growth phenomena on single crystal substrates.

Stranski-Krastanow (SK) growth, one of the three primary thin film growth modes, is generally used to describe a layer-by-layer thin film and subsequent island growth in a heteroepitaxial system.[30] The SK mode can predict the critical thickness of a coherent thin film growing on heterogeneous substrates.[31] The dislocation free SK growth was later reported by Eaglesham et al. showing a growth of Ge islands on Si with a critical thickness of ~50 nm.[32] The local elastic deformation around the island was considered to accommodate the strain energy in the islands. Owing to the similarity of the NW growth to above heteroepitaxial growth, the SK mode would be able to provide a general platform for better understanding of the epitaxial growth phenomena of NWs on heterogeneous substrates.

In this letter, we adapted the SK mode to the heteroepitaxial growth of NWs and suggested three general growth modes covering all phenomena observed from nanostructures epitaxially grown on substrates. Such growth modes were defined by a strain versus dislocation (SVD) model and supported by our large number of experimental observations. The SVD model describes the competition between the strain energy and dislocation energy at the interface between the NW and substrate. This model has been successfully applied to explain the growth behaviors of ZnO NWs and nanofins on GaN and sapphire substrates.

2. Experimental Section

Synthesis of ZnO Nanowires and Nanofins. A horizontal hot wall tube furnace was used to perform the vapor deposition of ZnO nanowires and nanofins on GaN and sapphire substrates. Prior to growth, for nanowire synthesis, a uniformly thin gold film was made on the GaN and sapphire substrates; for nanofin fabrication, patterned thin gold film was made on these substrates from a photolithographic process. Different sizes of

* Corresponding author. E-mail: xudong@engr.wisc.edu.

10.1021/jp910464p
Published on Web 01/13/2010

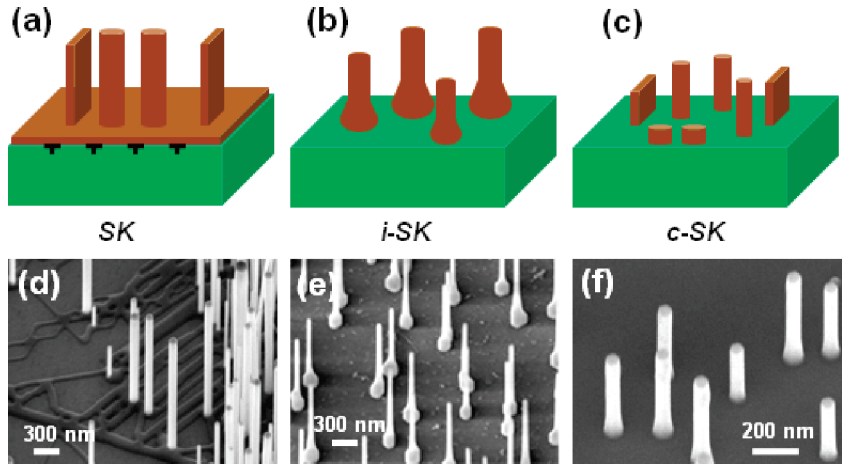

Figure 1. Three suggested heteroepitaxial growth modes of NWs. (a) The SK mode, where a defective film forms between the solid substrate and strain-free NWs. (b) The island SK (*i*-SK) mode, where a cone-shaped base forms beneath the NW. (c) The coherent SK (*c*-SK) mode, where dislocation-free NWs directly grows on the substrate surface without any intermediate structure. (d−f) Typical SEM images showing ZnO NWs grown on GaN substrate via the SK, *i*-SK, and *c*-SK modes, respectively.

quartz tube supporting the precursors and substrates were applied to produce varieties of vapor concentrations. The typical dimension of the quartz tubes are 25 cm in length and 1.6 cm in inner diameter; 25 cm in length and 2.0 cm in inner diameter; and 40 cm in length and 1.6 cm in inner diameter, and so on. In a typical process, 0.3 g ZnO powder and 0.3 g graphite powder were mixed and grounded together and placed in a 3 cm long quartz boat positioned 5 cm from one end in the quartz tube. Four or five pieces of GaN epi-layer on sapphire and a-plane sapphire substrates were placed inside the quartz tube, where the first substrate was 8 cm from the source boat and the rests were farther from the source and 3 cm from each other. Then we placed the small quartz tube into the large alumina tube in the tube furnace. Source boat was aligned at the center of the furnace and these substrates located on the downstream side of carrier gas. The carrier gas used in the experiments was 1% oxygen mixed by high purity argon. First, the furnace was quickly increased to 925 °C at a ramp rate of 50 °C/min. When the temperature reached 400 °C, the carrier gas was introduced into the chamber with a flow rate of 50 sccm. By tuning the controlling valve, a 20 Torr system pressure was kept. Then we held the furnace temperature at 925 °C for 30 min. Different growth conditions were applied by changing the growth temperatures and flow rates, respectively. Finally, the furnace was turned off and cooled down naturally without changing the system pressure and carrier gas flow rates.

Characterization. The products were characterized by FESEM (LEO 1530) and high resolution TEM (Philips CM 200).

3. Result and Discussion

3.1. Three Modes of Nanowire Heteroepitaxial Growth. For NWs growing epitaxially on heterogeneous substrates, three growth behaviors were typically observed. First, NWs can grow vertically on a thin film formed by the same material on top of the substrate (Figure 1a). This film serves as a buffer layer and NWs growing above could thus be considered as a homoepitaxial growth. The high density of nucleation sites due to dense catalysts and high vapor concentration is believed to be the main reason for the formation of this film. Figure 1d shows such a situation where vertical ZnO NWs grew on a very thin layer of ZnO network. The size of these NWs has a wide distribution. In addition, the Au catalyst droplets can be clearly seen on top of these NWs, indicating the NWs were formed via a vapor−liquid−solid (VLS) process. Similar growth behavior has also been found in the formation of In_2O_3 NWs on sapphire substrates.[33] We also discovered that most vertically aligned ZnO NWs synthesized by vapor deposition belong to this mode: a more or less thick defective ZnO thin film always presented beneath the vertical strain-free ZnO NWs. As schematically shown in Figure 1a, we simply used misfit dislocations to represent the complicated defects of the thin films. Due to the appearance of a defective heteroepitaxial thin film (or continuous network) prior to the NW formation, this growth behavior is attributed to the general SK mode.

Under some other situations, a big cone-shape base would form beneath a long, vertical ZnO NW with uniform thickness (Figure 1b). Experimental observation showed that the size and size distribution of the NWs in this category were smaller than the NWs from the SK mode. This was a common phenomenon when vertically aligned NWs were grown discretely from each other (Figure 1e). Similar to the continuous film, the large base beneath the NW may also contain dislocations to reduce the misfit strain energy at the interface. Therefore, this behavior is defined as the island SK (*i*-SK) mode. A least happened phenomenon is that vertical NWs grow on bare substrate surface without any transition structures (Figure 1c). Figure 1f shows that these types of NWs had the smallest average size and a narrow size distribution. Similarly, Au catalyst droplets can be observed on the top of these NWs indicating a VLS growth process, too. NWs with such small sizes were generally discovered dislocation free. Accordingly, this growth behavior is defined as the coherent SK (*c*-SK) mode. The SK, *i*-SK and *c*-SK modes would cover all the growth phenomena when vertical NWs were grown epitaxially on heterogeneous substrates. Among them, the *c*-SK mode is mostly desired due to the uniform dimension of each NW and the overall narrower size distribution.

3.2. Prediction of NW Growth Behaviors by Strain versus Dislocation Model. To apply these three modes to predict and design the heteroepitaxial growth behaviors of NWs, a theoretical framework was established based on the strain and dislocation energies existing at the NW-substrate interface, the SVD model. Several important assumptions for this model are listed below:

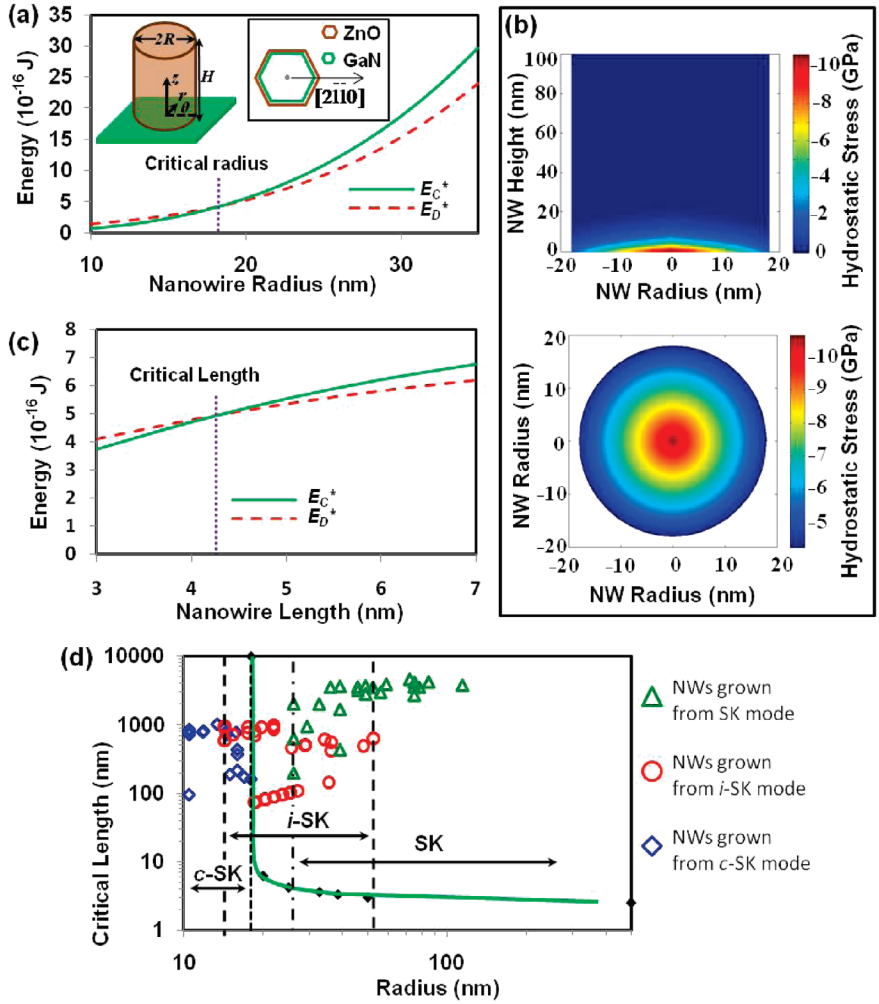

Figure 2. SVD model used to calculate the ZnO-NWs-on-GaN-substrate system. (a) Energy vs NW radius plot for comparing the coherent energy (E_C*) and the energy with dislocation (E_D*) of a NW with an infinite length, where an 18 nm critical radius of the ZnO NW is determined. Left inset is the heteroepitaxial NW model used in the calculation. Right inset shows the epitaxial relationship between ZnO and GaN. (b) Hydrostatic stress distribution along a NW that is 36 nm in diameter (top) and on the NW-substrate interface (bottom). (c) Energy vs NW length plot for comparing E_C* and E_D* of a NW with a radius of 25 nm, where a 4.2 nm critical length is determined. (d) Critical length vs radius plot of dislocation free ZnO NWs. Triangle, circle, and diamond markers are experimental data measured from ZnO NWs grown on GaN substrate via SK, *i*-SK, and *c*-SK modes, respectively.

(1) The NW array has a moderate density, where the distances among NWs are much larger than their radii. This is a common case for most vertically aligned NWs growing directly from the substrate. Therefore, the strain energy interaction among neighboring NWs is trivial and will not be considered in our model.

(2) The lattice of substrate is rigid along the radial direction, while the NW-substrate interface is deformable out of the plane. A curved interface to accommodate the strain energy is very likely to occur when a small lattice mismatch is presented.[32,34] On the other hand, based on the fact that the lattice of small sized NWs is much less restrictive to deformation comparing to the bulky substrate surface, the interface mismatch energy would be largely compensated by the deformation of NW. Therefore, we consider the curved interface energy and the lattice mismatch energy in the NW as the total energy of the heteroepitaxial system.

(3) The NWs are dislocation free. Appearance of dislocation would favor a lateral growth of thin film, network, or big bases and suppress the NW growth initially. Therefore, we apply this assumption as a criterion for determining the formation of NW structure via *c*-SK mode.

(4) Two perpendicularly pure edge dislocations are presented to reduce the strain energy. This is a general and fairly close approximation of energy releasing mechanism in heteroepitaxial growth systems, which has been successfully applied to island geometries[35] and NW heterostructure systems.[27]

(5) The thermoelastic strain is neglected in the SVD model. In the ZnO/GaN heteroepitaxial growth system at 925 °C, the thermoelastic strain was estimated to be 0.025%, which is only one percent of the mismatch strain.[36]

Based upon above assumptions, the coherent strain energy and the energy when the first pair of dislocations appears were calculated as functions of NW's length and radius, respectively. The point where these two energies intersect was defined as the critical size of coherently grown NWs. Following calculations were all based on ZnO nanostructures but they are completely adaptable to other crystal systems.

The ZnO-NW-on-GaN-substrate system is schematically shown in the left inset of Figure 2a. The ZnO NW grew along the [0001] direction (the *z*-axis) with the interface at $z = 0$. The height of the NW was defined as H and the radius of the unstrained NW was R. A cylindrical coordinate was applied to calculate the energies of continuum and dislocated systems. The

lattice relation is illustrated in the right inset of Figure 2a, where the ZnO NW was compressed since the lattice constant of ZnO is 2% larger than GaN along the <2$\bar{1}\bar{1}$0> directions.

The increasing of the NW's diameter could induce an increment of the elastic energy due to lattice mismatch (f). Ultimately, a pair of misfit dislocations will be generated to lower the strain energy. Apparently, there is a critical value reflecting the appearance of the first pair of dislocations. Thus, both R and H would have a critical value, for example, critical radius (R^*) when the length is infinite and critical length (H^*) at certain radius. To determine the critical values, the total strain energy in a coherent NW heterostructure (E_C) was compared to the total energy of a dislocated NW heterostructure (E_D), which includes the dislocation energy and the residual strain energy. The point where E_D became smaller than E_C gave the critical value of the system. The interactions between the dislocations and the mismatch strain fields were ignored.

A uniformly stretched displacement along the radial direction and an exponential decay along the z-axis were assumed

$$\begin{aligned} u_r(r,\theta,z) &= Br\exp\left(\frac{-z}{2\alpha R}\right) \\ u_\theta(r,\theta,z) &= 0 \\ u_z(r,\theta,z) &= (Pr+QR)\exp\left(\frac{-z}{2\alpha R}\right) \end{aligned} \tag{1}$$

where B represents how much the NW lattice distortion is needed to eliminate the lattice mismatch, here $B = f$ because the substrate is rigid; α is a constant reflecting the strain energy relaxation along the z-axis; and constants P and Q are related to the deformation of the interface. Minimum potential energy approach was used to determine the strain energy of NW and the three unknown constants α, P, and Q.[27]

Based on the relationship between displacement and strain, the expression of strain in a cylindrical coordinate can be written as

$$\begin{aligned} \varepsilon_{rr} &= B\exp\left(\frac{-z}{2\alpha R}\right) \\ \varepsilon_{\theta\theta} &= B\exp\left(\frac{-z}{2\alpha R}\right) \\ \varepsilon_{zz} &= -\frac{Pr+QR}{2\alpha R}\exp\left(\frac{-z}{2\alpha R}\right) \\ \varepsilon_{rz} &= \frac{-Br+2PR\alpha}{4\alpha R}\exp\left(\frac{-z}{2\alpha R}\right) \\ \varepsilon_{r\theta} &= 0 \\ \varepsilon_{z\theta} &= 0 \end{aligned} \tag{2}$$

According to Hooke's law, the stress is

$$[\sigma] = [C][\varepsilon] = \begin{pmatrix} C_{11}\varepsilon_{rr}+C_{12}\varepsilon_{\theta\theta}+C_{13}\varepsilon_{zz} \\ C_{12}\varepsilon_{rr}+C_{12}\varepsilon_{\theta\theta}+C_{13}\varepsilon_{zz} \\ C_{13}\varepsilon_{rr}+C_{13}\varepsilon_{\theta\theta}+C_{33}\varepsilon_{zz} \\ 0 \\ 2C_{44}\varepsilon_{zr} \\ 0 \end{pmatrix} \tag{3}$$

where $[C]$ is the stiffness matrix obtained from ref 37. The hydrostatic stress distributions along the NW and on the NW-substrate interface are shown in Figure 2b. It can be seen that the highest stress exists at the center of the NW and gradually decreases along the radius direction. The stress usually disappears at ~20 nm above the interface.

The strain energy density can then be expressed as

$$e(r,\theta,z) = \frac{1}{2}\sigma_{ij}\varepsilon_{ij} \tag{4}$$

Thus, integrating the strain energy density gives the total strain energy of the system:

$$\begin{aligned} E_C = \int_0^H\int_0^{2\pi}\int_0^R e(r,\theta,z)r\mathrm{d}r\mathrm{d}\theta\mathrm{d}z = \frac{\pi R^3}{96\alpha}[(48C_{11}B^2 + \\ 144C_{12}B^2 + 48C_{44}P^2)\alpha^2 + (-96C_{13}BQ - 64C_{13}BP - \\ 32C_{44}BP)\alpha + 12C_{33}Q^2 + 8C_{33}PQ + 6C_{33}P^2 + \\ 6C_{44}B^2]\left[1 - \exp\left(\frac{-H}{\alpha R}\right)\right] \end{aligned} \tag{5}$$

The strain energy expression is dependent on the constants α, P, and Q. In an equilibrium system, E_C is minimized. We used a numerical method to reveal the minimum value, which would be the total strain energy of the NW. Detailed process can be found in the Supporting Information (S1). For instance, for an infinite long ZnO NW with a radius of 20 nm, the strain energy was found to be 4.2×10^{-16} J. The constants α, P, and Q were 0.1349, −0.0064, and −0.0033, respectively.

In calculating the total energy of the plastically deformed system, the core energy and the strain energy that was partially relaxed by the pure edge misfit dislocations were considered. A pair of perpendicularly pure edge dislocations were assumed to appear along the $[2\bar{1}\bar{1}0]_{ZnO}$ and $[01\bar{1}0]_{ZnO}$ directions, respectively. Based on Matthew's model,[31] the total energy of the two edge dislocations is given by:

$$E_d = 2\times 2R\frac{Gb^2}{4\pi(1-\upsilon)}\left(\ln\frac{\bar{h}}{b}+1\right) \tag{6}$$

R is the radius of the NW, G is the shear modulus, b is value of burger's vector, and $\bar{h}$ is the nearest distance between the dislocation and a free surface. G was calculated from the stiffness constant shown in Supporting Information (S2). Following relationships were established based on Ovidko's method and Glas' extension[28]

$$\begin{aligned} \bar{h} &= H \quad \text{if} \quad H \le \beta R \\ \bar{h} &= \beta R \quad \text{if} \quad H > \beta R \end{aligned} \tag{7}$$

where $\beta = 2/\pi$ is used to modify the shape of the wire. As defined previously, the total energy of the dislocated system is

$$E_D = E_{res} + E_d \tag{8}$$

where E_{res} is the residual strain energy, which can be acquired through the same procedure of a coherent system but with reduced lattice mismatch (f_{res}). Due to the relaxation from the pure edge dislocations, f_{res} is given by

$$|f_{res}| = |f| - |\varepsilon_d| = |f| - \left|\frac{b}{2R}\right|; \quad (0 \le b \le 2Rf) \tag{9}$$

Finding the values of α, P, and Q in eq 1 gives the minimum strain energy of a coherent system (E_C*), and the minimum residual strain energy of a dislocated system (E_{res}*). Thus, the minimum total energy of a dislocated system is $E_D^* = E_{res}^* + E_d$. Equations 5 and 6 demonstrate both E_C* and E_D* are functions of the NW's radius (R) and length (H). Their relationships to R are plotted in Figure 2a for NWs with infinite length. When R is small, the strain energy of a coherent system is lower than the total energy of a dislocated system, for example, $E_C^* < E_D^*$. When R becomes larger, E_C* increases faster than E_D* and eventually becomes more significant. The radius where these two energies intersect was defined as the critical radius (R*). Ideally, dislocation-free NWs with an infinite length could only be formed with a radius smaller than R*. For the ZnO NW on GaN substrate system, R* was found to be 18 nm as shown in Figure 2a.

Increasing the radius of a dislocation-free NW would significantly increase the coherent energy, thus, reducing the critical length of the NW. With a given radius, the two competitive energies, E_C* and E_D*, were calculated as a function of the NW's length via eqs 5 and 6. The critical length was therefore determined from the intersection point of these two energies. Figure 2c shows the energy versus length curves for a NW with a radius of 25 nm, where a 4.2 nm critical length was obtained. This result suggested that if a 50 nm wide dislocation-free ZnO NW should be grown on a GaN substrate via the c-SK mode, it could only reach 4.2 nm long. This clearly showed that the lateral relaxation around the NWs played a dominant role in determining the length of a coherent NW on heterogeneous substrates.

The process shown in Figure 2c revealed how tall a dislocation-free NW could grow at a given radius. Repeating this process at different radii generated a series of points that defined the critical length to radius (H^*-R) relationship, which was shown by the solid diamond markers in Figure 2d. The critical length quickly jumped from a few nanometers to infinity when the NW's radius approached its critical radius. The curve generated by those points could be used to predict the growth behaviors and NW dimensions. To reveal how the H^*-R curve was related to the three growth modes, lengths and radii were measured from ZnO NWs synthesized from various experimental batches and plotted together with the curve (Figure 2d). The diamond markers represent data measured from ZnO NWs grown via c-SK mode. All the c-SK-grown NWs lie on the left hand side of the curve. This demonstrated that our SVD model is able to predict the critical size of dislocation-free NWs that are vertically and uniformly grown on heterogeneous substrates.

The i-SK grown NWs were marked as circles in the plot. They exhibited larger size and distributed on both sides of the H^*-R curve. The increasing of the NW size indicates the base formed under those NWs could largely release the interfacial strain energy, thus, provide a nearly strain-free homoeptiaxial growth platform. For the NWs grown via SK mode, both their size and distribution were larger than the ones from c-SK and i-SK modes. This observation strongly supported our statement that the underneath defective film accommodates all the compressive strain, thus, NWs could grow with an "unlimited" length and width. In reality, under this circumstance, the size of NWs will be controlled by catalysts or thermodynamic parameters. The relationship between the growth modes and the H^*-R curve clearly showed that the SVD model was properly established and could serve as effective guidance for designing vertically aligned NWs on heterogeneous substrates.

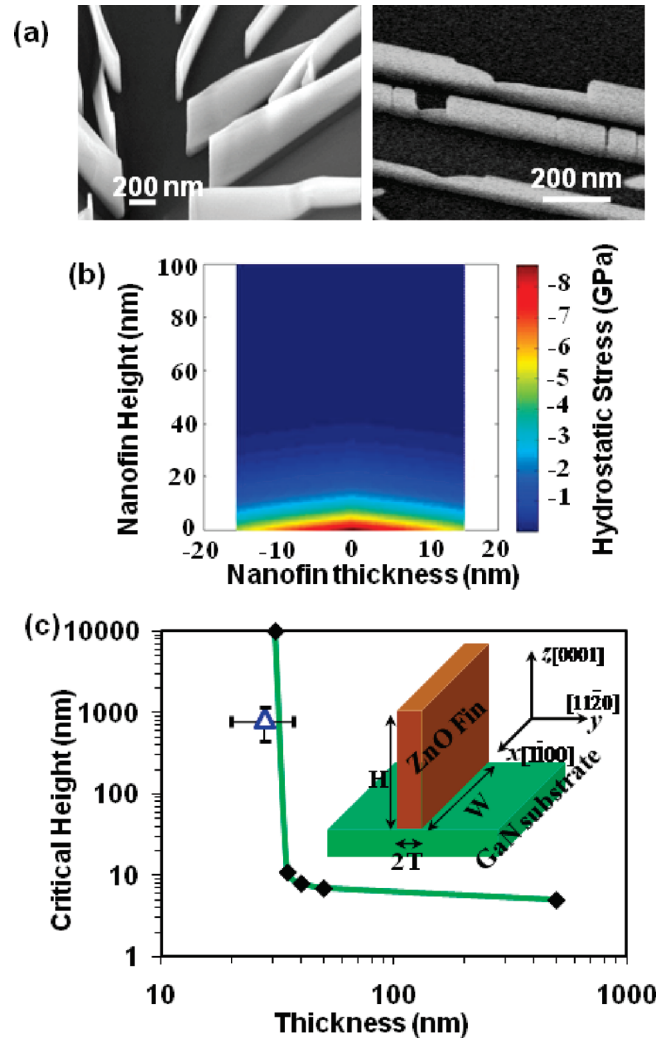

Figure 3. SVD model to calculate the ZnO-nanofins-on-GaN-substrate system. (a) SEM images of ZnO nanofin structures growing on ZnO buffer layer (left), and on GaN substrate (right). (b) Hydrostatic stress distribution along a nanofin structure that is 31 nm in thickness. (c) Critical height vs thickness plot of ZnO nanofins. The averaged experiment data is presented by the triangular symbol. Inset shows a schematic configuration of a ZnO nanofin grown on GaN substrate, where the nanofin's thickness, width, and height are defined as $2T$, W, and H, respectively.

3.3. Prediction of Nanofin Growth Behaviors by Strain versus Dislocation Model. The SVD model could also be applied to other heteroepitaxial nanostructures, such as nanofins or nanowalls.[38] Typical nanofin structures are shown in Figure 3a. Image on the left hand side shows ZnO nanofins grown on ZnO buffer layer, where no lattice mismatch was presented. They can be included in the SK mode, where the nanofins can be grown tall and wide. Image on the right hand side shows ZnO nanofins grown on GaN substrate, which fell in the category of the c-SK mode. In such a nanofin structure, the hydrostatic stress distribution along the cross-section normal to the substrate is shown in Figure 3b. Similar to NWs, highest stress exists at the center of the nanofin, while it disappears at ~40 nm above the interface. Different from NWs, such 2D nanostructures have one more dimension that needs to be considered as infinite (the width dimension W as shown in the inset of Figure 3c). It has been found that, along this direction, a series of amorphous holes (~5 nm in diameter, perpendicular to the width direction) usually appears to release the strain energy along the this direction.[39] Therefore, to predict the critical

size of the ZnO nanofins on GaN substrate, we assumed the strain along the width direction was completely released and only considered the strain energy along the thickness direction. The detailed derivation is included in the Supporting Information (S4). In Figure 3c, the plot was acquired by the same method as that of NWs. The critical thickness (defined as $2T$) was found to be 31 nm for ZnO nanofins grown on GaN substrate. Multiple nanofin structures were measured from different synthesis batches, and the average thickness and height were 28 ± 8 nm and 900 ± 400 nm, respectively, as presented by the triangular marker in Figure 3c. This observation fell within the allowed region predicted by the calculation, which successfully showed that the SVD model can be easily adapted to other nanostructure systems.

3.4. Prediction of Nanostructures Growth on Sapphire by Strain versus Dislocation Model. To further illustrate the SVD model for predicting nanostructure growth, we also grew and calculated the growth behaviors of ZnO nanostructures on sapphire substrates. Experimentally, vertically aligned ZnO NWs could not possibly be grown via the *c*-SK mode on sapphire. On the other hand, ZnO NWs with underneath defective film could always be found on sapphire, indicating the SK growth mode was dominating. Nanofin appeared to be an impossible morphology on sapphire; instead, only horizontal NWs could be received. Consistent misfit dislocations have been revealed within such horizontal NWs. To explain these observations, we adopt the SVD model to describe the ZnO−sapphire system. As shown in Figure 4a, *a*-plane sapphire is usually used for growing *c*-plane orientated ZnO. The in-plane pseudo lattice mismatch between ZnO and sapphire is 0.1 and 2.3% along the $<11\bar{2}0>_{ZnO}||\langle 0001\rangle_{Al_2O_3}$ and $<1\bar{1}00>_{ZnO}||<1\bar{1}00>_{Al_2O_3}$ directions, respectively. However, experimental observations have demonstrated that the pseudo lattice mismatch could not effectively define the NW growth behavior. A significantly out of plane compressive strain (7%) has been discovered on the (0001) plane of ZnO nanostructures grown on sapphire substrate.[34] Thus, based on the Poisson's effect, the real lattice mismatch should be conservatively assumed to be ~20% between the $(11\bar{2}0)_{ZnO}$ and $(0003)_{Al_2O_3}$. A tetragonal structure of ZnO NWs was also assumed for simplification. The calculation was based on a ZnO NW or a nanofin with a thickness ($2T$) of 40 nm, which was a typical observed size. The detail calculation is included in the Supporting Information (S3 and S4). Figure 4b compares the strain energy of a coherent NW system and the total energy of a dislocated NW system, where these two curves never intersect. This indicated that the *c*-SK mode is energetically unfavorable for ZnO NWs to grow on sapphire substrates. In other words, to grow vertically aligned ZnO NWs on sapphire substrates, a defective film (SK mode) or a large defective individual base (*i*-SK mode) is always required. This conclusion matched our experiment observations. It also explained the growth condition window for synthesizing vertically aligned ZnO NWs on sapphire substrates is much smaller than that of GaN substrates, because the deposition condition has to satisfy both film and NW growth in a ZnO−sapphire system.

For the ZnO-nanofin-on-sapphire system, it was assumed that the 20% lattice mismatch between ZnO $(11\bar{2}0)$ and sapphire (0003) contributed the most strain energy to the system. As shown in Figure 4c, the E_C* term is always larger than E_D*, demonstrating the dislocation-free nanofin structure is energetically unfavorable in the ZnO−sapphire system. If lateral growth should appear, the height would be restricted at a very small value with misfit dislocations. Thus, only horizontal NWs can be formed in such a system (inset of Figure 4c).

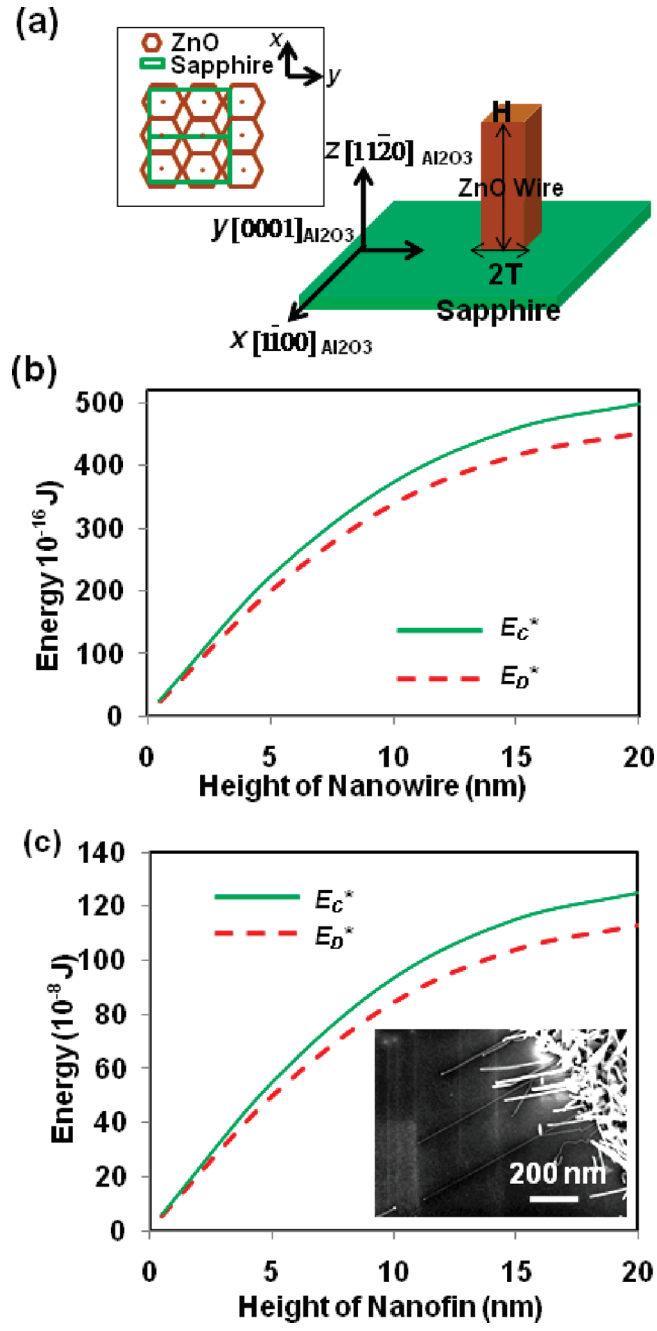

Figure 4. SVD model to calculate the ZnO-NWs-on-sapphire-substrate system. (a) A schematic of a ZnO NW grown on sapphire substrate, where a tetragonal shape ZnO NW was assumed. Inset shows the epitaxial relationships between *c*-plane ZnO and *a*-plane sapphire. (b) Energy vs NW length plot for comparing the coherent energy (E_C*) and the energy with dislocation (E_D*) of a NW with a thickness of 40 nm. (c) Energy vs nanofin length plot for comparing the E_C* and E_D* of a nanofin with a thickness of 40 nm. Neither of the curves intersects in plot (b) and (c) indicating coherent growth is not a favorable mode for the ZnO−sapphire system.

4. Conclusions

In summary, based on the SK thin film growth mode, we suggested SK, *i*-SK, and *c*-SK, three NW growth modes that generalize and explain all the growth behaviors of heteroepitaxial NWs on single crystal substrates. The suggested modes were defined by the SVD model that compares strain energy and dislocation energy at the NW-substrate interface. Experimental data acquired from ZnO NWs grown on GaN substrates via the three modes exhibited a good match to our theoretical prediction.

The SVD model has also been successfully applied to ZnO nanofin structures grown on GaN and ZnO nanostructures grown on sapphire, which demonstrated the generality of the SVD model for understanding the heteroepitaxial growth behaviors of various nanostructures. This work provided a necessary quantitative complement to the thermodynamics and diffusion kinetics in interpreting the nanostructure growth phenomena. This work could be applied to guide the interface engineering in nanostructure and nanodevice fabrication, as well as to predict the size, morphology, and even quality of desired nanostructures.

Acknowledgment. This work was supported by the National Science Foundation under Grant Nos. DMR-0905914 and CMMI-0926245.

Supporting Information Available: Strain energy of ZnO nanowire on GaN substrate; Shear modulus of ZnO nanowire; Strain Energy of ZnO nanowire on sapphire substrates; and Strain energy of ZnO nanofin on GaN and sapphire. This material is available free of charge via the Internet at http://pubs.acs.org.

References and Notes

(1) Park, W. I.; Yi, G. C. *Adv. Mater.* **2004**, *16*, 87.
(2) Qian, F.; Gradecak, S.; Li, Y.; Wen, C. Y.; Lieber, C. M. *Nano Lett.* **2005**, *5*, 2287.
(3) Huang, M. H.; Mao, S.; Feick, H.; Yan, H. Q.; Wu, Y. Y.; Kind, H.; Weber, E.; Russo, R.; Yang, P. D. *Science* **2001**, *292*, 1897.
(4) Agarwal, R.; Barrelet, C. J.; Lieber, C. M. *Nano Lett.* **2005**, *5*, 917.
(5) Xiang, J.; Lu, W.; Hu, Y. J.; Wu, Y.; Yan, H.; Lieber, C. M. *Nature* **2006**, *441*, 489.
(6) Patolsky, F.; Timko, B. P.; Yu, G. H.; Fang, Y.; Greytak, A. B.; Zheng, G. F.; Lieber, C. M. *Science* **2006**, *313*, 1100.
(7) Ferry, D. K. *Science* **2008**, *319*, 579.
(8) Bryllert, T.; Wernersson, L. E.; Froberg, L. E.; Samuelson, L. *IEEE Electron Device Lett.* **2006**, *27*, 323.
(9) Wang, X. D.; Summers, C. J.; Wang, Z. L. *Nano Lett.* **2004**, *4*, 423.
(10) Cui, Y.; Wei, Q. Q.; Park, H. K.; Lieber, C. M. *Science* **2001**, *293*, 1289.
(11) Gratzel, M. *Nature* **2001**, *414*, 338.
(12) Law, M.; Greene, L. E.; Johnson, J. C.; Saykally, R.; Yang, P. D. *Nat. Mater.* **2005**, *4*, 455.
(13) Wang, X. D.; Song, J. H.; Liu, J.; Wang, Z. L. *Science* **2007**, *316*, 102.
(14) Qin, Y.; Wang, X. D.; Wang, Z. L. *Nature* **2008**, *451*, 809.
(15) Kuykendall, T.; Pauzauskie, P. J.; Zhang, Y. F.; Goldberger, J.; Sirbuly, D.; Denlinger, J.; Yang, P. D. *Nat. Mater.* **2004**, *3*, 524.
(16) Martensson, T.; Svensson, C. P. T.; Wacaser, B. A.; Larsson, M. W.; Seifert, W.; Deppert, K.; Gustafsson, A.; Wallenberg, L. R.; Samuelson, L. *Nano Lett.* **2004**, *4*, 1987.
(17) Wei, W.; Bao, X. Y.; Soci, C.; Ding, Y.; Wang, Z. L.; Wang, D. *Nano Lett.* **2009**, *9*, 2926.
(18) Wang, X. D.; Song, J. H.; Li, P.; Ryou, J. H.; Dupuis, R. D.; Summers, C. J.; Wang, Z. L. *J. Am. Chem. Soc.* **2005**, *127*, 7920.
(19) Paetzelt, H.; Gottschalch, V.; Bauer, J.; Benndorf, G.; Wagner, G. *J. Cryst. Growth* **2008**, *310*, 5093.
(20) Lei, M.; Yang, H.; Li, P. G.; Tang, W. H. *Appl. Surf. Sci.* **2008**, *254*, 1947.
(21) Gudiksen, M. S.; Wang, J. F.; Lieiber, C. M. *J. Phys. Chem. B* **2001**, *105*, 4062.
(22) Hannon, J. B.; Kodambaka, S.; Ross, F. M.; Tromp, R. M. *Nature* **2006**, *440*, 69.
(23) Wang, X. D.; Song, J. H.; Summers, C. J.; Ryou, J. H.; Li, P.; Dupuis, R. D.; Wang, Z. L. *J. Phys. Chem. B* **2006**, *110*, 7720.
(24) Borgstrom, M. T.; Immink, G.; Ketelaars, B.; Algra, R.; Bakkers, E. P. A. M. *Nat. Nanotechnol.* **2007**, *2*, 541.
(25) Jensen, L. E.; Bjork, M. T.; Jeppesen, S.; Persson, A. I.; Ohlsson, B. J.; Samuelson, L. *Nano Lett.* **2004**, *4*, 1961.
(26) Levin, I.; Davydov, A.; Nikoobakht, B.; Sanford, N.; Mogilevsky, P. *Appl. Phys. Lett.* **2005**, *87*, 103110.
(27) Ertekin, E.; Greaney, P. A.; Chrzan, D. C.; Sands, T. D. *J. Appl. Phys.* **2005**, *97*, 114325.
(28) Glas, F. *Phys. Rev. B* **2006**, *74*, 121302.
(29) Ye, H.; Lu, P. F.; Yu, Z. Y.; Song, Y. X.; Wang, D. L.; Wang, S. M. *Nano Lett.* **2009**, *9*, 1921.
(30) Stranski, I. N.; Krastanow, L. *Akad. Wiss. Lit. Mainz Math.-Natur. Kl. IIb* **1939**, *146*, 797.
(31) Matthews, J. W. *J. Vac. Sci. Technol.* **1975**, *12*, 126.
(32) Eaglesham, D. J.; Cerullo, M. *Phys. Rev. Lett.* **1990**, *64*, 1943.
(33) Nguyen, P.; Ng, H. T.; Yamada, T.; Smith, M. K.; Li, J.; Han, J.; Meyyappan, M. *Nano Lett.* **2004**, *4*, 651.
(34) Nikoobakht, B.; Eustis, S.; Herzing, A. *J. Phys. Chem. C* **2009**, *113*, 7031.
(35) Cabrera, N. *Surf. Sci.* **1964**, *2*, 320.
(36) Kumar, V.; Sastry, B. S. R. *Cryst. Res. Technol.* **2001**, *36*, 565.
(37) Azuhata, T.; Takesada, M.; Yagi, T.; Shikanai, A.; Chichibu, S.; Torii, K.; Nakamura, A.; Sota, T.; Cantwell, G.; Eason, D. B.; Litton, C. W. *J. Appl. Phys.* **2003**, *94*, 968.
(38) Shi, J.; Grutzik, S.; Wang, X. D. *ACS Nano* **2009**, *3*, 1594.
(39) Wang, X. D.; Ding, Y.; Li, Z.; Song, J. H.; Wang, Z. L. *J. Phys. Chem. C* **2009**, *113*, 1791.

JP910464P